CHANGE OF OPTICAL AND MICROPHYSICAL PROPERTIES OF AEROSOLS DURING DIFFUSION AND SEDIMENTATION SPREAD OF ANOMALOUS AEROSOL LAYERS IN THE MESOSPHERE

R.F. Rakhimov

Institute of Atmospheric Optics,
Siberian Branch of the Russian Academy of Sciences, Tomsk
Received December 25, 1994

Model estimates are presented for optical and microphysical changes in aerosol constituent due to turbulent mixing and gravitational sedimentation of extraterrestrial particles. Corresponding variations in lidar ratio are shown to reach 300–400%, mostly because of the dynamics of changes in coarse aerosol fraction with altitude.

Unlike the stratospheric layer, our understanding of the nature of the mesospheric layer is still too limited. Along with substantial uncertainty of estimates about the rate of the extraterrestrial dust inflow to the layer,[1,2] quite little is known about the aerosol sinks and transformation mechanisms there. Aerosol instability due to sedimentation variations in the layer is further enhanced by a relatively strong turbulent mixing ($D \sim 3$–5 m^2/s).

Large extraterrestrial dust particles and micrometeors, entering the atmosphere, during their subsequent hard braking and heating, experience fragmentation, as well as vaporization, thus being an additional source of aerosol at these altitudes (80–110 km). Despite its significance, the diffusion-sedimentation spread of the injected aerosol anomalies, and the accompanying change of the optical and microphysical properties of the extraterrestrial aerosol at mesospheric altitudes, are still poorly represented in scientific literature.

Based on the fraction-by-fraction synthesis of the resultant particle size-distribution we consider in this paper spatiotemporal variations in the disperse structure of mesospheric aerosols by analyzing dynamics of variations of integrated size spectrum parameters.

To describe mathematically the structural changes in the layer, we started with a system of equations for components of vector parameter $\hat{Q}_i = \{N_i, S_i, V_i\}$, characterizing the aerosol size spectrum of the ith fraction in terms of lognormal distribution,[3,4]

$$\frac{\partial \hat{Q}_i(z, t)}{\partial t} = \frac{\partial}{\partial z} D(z) \frac{\partial \hat{Q}_i(z, t)}{\partial z} - \frac{\partial}{\partial t} [W_{qi}(z, t)\, \hat{Q}_i(z, t)], \quad (1)$$

where meant by the vector parameter $\hat{Q}_i(z, t)$ in ith equation may be either volume concentration, V_i, or surface concentration, S_i, or simply number density, N_i, of aerosol particles at an altitude z, t is the current time, W_{qi} is the mean Stokes sedimentation rate of particles of the ith fraction, which is evaluated, for each equation, from size spectrum according to the modal radius of the distribution density function of the corresponding integrated characteristic. The gravitational sedimentation rate is defined by the Stokes-Kanninhem formula[5] as

$$W_s = \frac{2 g \rho r^2}{9\eta} (1 + C_{K\,hi} K_n), \quad (2)$$

where r is the particle radius, g is the acceleration of gravity, ρ is the aerosol particle density, η is the viscosity of air, $K_n = l/r$ is the Knudsen constant, l_0 is the molecule free path, and $C_{K\,hi}$ is the Kanninhem correction factor weighted and averaged over the size spectrum of the ith fraction,[5]

$$C_{K\,hi} = 1 + \frac{l_0}{r_i} \left(1.257 + 0.4 \exp\left(-1.1 \frac{l_0}{r_i}\right)\right). \quad (3)$$

By assuming that the free path of air molecules l_0 obeys the barometric law of variation with height at a constant with height temperature T, we can readily generalize the expression for the sedimentation rate according to Ref. 9 as follows

$$W_s = \frac{2 g \rho r^2}{9\eta} - \frac{2 g \rho r}{9\eta} C_{K\,hi}\, l_0 \exp\left(\frac{m g z}{K_B T}\right) = -A - B \exp(\gamma z), \quad (4)$$

where m is the mass of air "molecule", K_B is the Boltzmann constant, l_0 is the air "molecule" free path under normal conditions.

Computation spans altitudes 76 to 116 km, between which the extraterrestrial dust is typically injected, while the meteorite particles being mostly fragmented and burnt.[7] Literature data available for these altitudes are as follows[6]: $T = 200$ K, $\eta = 1.7 \cdot 10^{-5}$ N·s/m^2; $l_0 = 4.2 \cdot 10^{-8}$ m; $\rho = 6.9 \cdot 10^3$ kg/m^3, with the latter number taken here as the most

0235-6880/95/09 663-04 $02.00

appropriate for the assumed chemical composition of the meteorite particles.

To avoid undesired confusion between the injected and background aerosol particle size spectra, the integrated parameters of the latter $\hat{Q}_i^b = \{N_i^b, S_i^b, V_i^b\}$ were assumed to vary with altitude exponentially, that is

$$\hat{Q}_i^b(z) = \hat{Q}_{i0}^b \exp\{-\hat{G}_{qi}^b (z - 72)\}, \quad (5)$$

where $\hat{Q}_{i0}^b$ is the integrated parameter of a background component at the height $z = 72$ km, while $\hat{G}_{qi}^b$ is the vector-parameter specifying the integrated parameter[1] vertical gradient. The $\hat{Q}_{i0}^b$ and $\hat{G}_{qi}^b$ values used in this paper are given in Table I.

TABLE I.

Fraction	N_{i0}^b, cm^{-3}	G_{ni}^b	S_{i0}^b, μm^2·cm^{-3}	G_{si}^b	V_{i0}^b, μm^3·cm^{-3}	G_{vi}^b
Accumu-lative	6.46E–2*	0.140	2.14E–3	0.143	5.11E–5	0.170
Coarse	6.41E–4	0.140	5.97E–4	0.158	7.59E–5	0.185

*Here and below, E–N abbreviates 10^{-N} (e.g., 6.46E–2 is equivalent to $6.46 \cdot 10^{-2}$).

Time computations of the micro and coarse fractions, injected into the anomalous layer started with the following integrated parameter values: $N_1 = 6.46\text{E}3$ cm^{-3}; $S_1 = 2.14\text{E}2$ μm^2 cm^{-3}; $V_1 = 5.11\text{E}0$ μm^3·cm^{-3}; $N_2 = 6.41\text{E}1$ cm^{-3}; $S_2 = 5.97\text{E}1$ μm^2·cm^{-3}; $V_2 = 7.59\text{E}0$ μm^3·cm^{-3}.

Time and space evolution of the model integrated parameters for the two aerosol fractions is illustrated in Tables II–IV.

TABLE II. Spatiotemporal evolution of aerosol constituent number densities.

z, km	Time, day			
	1.5	2.5	4.5	7.5
	N_1 (cm^{-3}) micro fraction			
76	0.797E–01	0.797E–01	0.797E–01	0.797E–01
80	0.455E–01	0.455E–01	0.455E–01	0.455E–01
84	0.260E–01	0.260E–01	0.260E–01	0.270E–01
88	0.149E–01	0.154E–01	0.362E–01	0.154E+00
92	0.529E+00	0.115E+01	0.183E+01	0.212E+01
96	0.603E+01	0.537E+01	0.442E+01	0.361E+01
100	0.714E–02	0.540E–01	0.303E+00	0.697E+00
104	0.158E–02	0.158E–02	0.217E–02	0.167E–01
108	0.903E–03	0.903E–03	0.903E–03	0.940E–03
112	0.516E–03	0.516E–03	0.516E–03	0.516E–03

TABLE II. (continued).

z, km	Time, day			
	1.5	2.5	4.5	7.5
	N_2 (cm^{-3}) coarse fraction			
76	0.178E–03	0.178E–03	0.178E–03	0.178E–03
80	0.102E–03	0.102E–03	0.102E–03	0.102E–03
84	0.582E–04	0.582E–04	0.582E–04	0.585E–04
88	0.333E–04	0.333E–04	0.348E–04	0.417E–04
92	0.388E–04	0.678E–04	0.991E–04	0.111E–03
96	0.247E–03	0.221E–03	0.182E–03	0.149E–03
100	0.625E–05	0.748E–05	0.157E–04	0.295E–04
104	0.354E–05	0.354E–05	0.355E–05	0.396E–05
108	0.202E–05	0.202E–05	0.202E–05	0.202E–05
112	0.116E–05	0.116E–05	0.116E–05	0.116E–05

TABLE III. Time evolution of altitude profile of the integrated particle surface.

z, km	Time, day			
	1.5	2.5	4.5	7.5
	S_1 (μm^2·cm^{-3}) micro fraction			
76	0.363E–02	0.363E–02	0.363E–02	0.363E–02
80	0.205E–02	0.205E–02	0.205E–02	0.205E–02
84	0.116E–02	0.116E–02	0.116E–02	0.117E–02
88	0.653E–03	0.662E–03	0.987E–03	0.277E–02
92	0.851E–02	0.176E–01	0.275E–01	0.316E–01
96	0.879E–01	0.783E–01	0.646E–01	0.528E–01
100	0.192E–03	0.912E–03	0.455E–02	0.102E–01
104	0.662E–04	0.662E–04	0.754E–04	0.289E–03
108	0.374E–04	0.374E–04	0.374E–04	0.379E–04
112	0.211E–04	0.211E–04	0.211E–04	0.211E–04
	S_2 (μm^2·cm^{-3}) coarse fraction			
76	0.116E–02	0.116E–02	0.116E–02	0.116E–02
80	0.615E–03	0.615E–03	0.615E–03	0.638E–03
84	0.327E–03	0.327E–03	0.344E–03	0.365E–03
88	0.175E–03	0.198E–03	0.232E–03	0.225E–03
92	0.219E–03	0.223E–03	0.200E–03	0.175E–03
96	0.175E–03	0.155E–03	0.130E–03	0.111E–03
100	0.261E–04	0.266E–04	0.293E–04	0.338E–04
104	0.139E–04	0.139E–04	0.139E–04	0.140E–04
108	0.737E–05	0.737E–05	0.737E–05	0.737E–05
112	0.392E–05	0.392E–05	0.392E–05	0.392E–05

TABLE IV. Time evolution of altitude profile of the integrated particle volume.

z, km	Time, day			
	1.5	2.5	4.5	7.5
	V_1 (μm^3·cm^{-3}) micro fraction			
76	0.192E–03	0.192E–03	0.192E–03	0.192E–03
80	0.971E–04	0.971E–04	0.971E–04	0.971E–04
84	0.492E–04	0.492E–04	0.492E–04	0.495E–04
88	0.249E–04	0.251E–04	0.311E–04	0.637E–04
92	0.164E–03	0.327E–03	0.502E–03	0.575E–03
96	0.157E–02	0.140E–02	0.115E–02	0.945E–03
100	0.467E–05	0.178E–04	0.825E–04	0.183E–03
104	0.164E–05	0.164E–05	0.181E–05	0.560E–05

TABLE IV. (continued).

z, km	Time, day			
	1.5	2.5	4.5	7.5
V_1 ($\mu m^3 \cdot cm^{-3}$) micro fraction				
108	0.832E–06	0.832E–06	0.832E–06	0.842E–06
112	0.421E–06	0.421E–06	0.421E–06	0.421E–06
V_2 ($\mu m^3 \cdot cm^{-3}$) coarse fraction				
76	0.602E–03	0.602E–03	0.602E–03	0.617E–03
80	0.287E–03	0.287E–03	0.301E–03	0.300E–03
84	0.137E–03	0.141E–03	0.159E–03	0.151E–03
88	0.797E–04	0.998E–04	0.877E–04	0.793E–04
92	0.842E–04	0.676E–04	0.525E–04	0.439E–04
96	0.301E–04	0.269E–04	0.233E–04	0.208E–04
100	0.710E–05	0.714E–05	0.735E–05	0.768E–05
104	0.339E–05	0.339E–05	0.339E–05	0.340E–05
108	0.162E–05	0.162E–05	0.162E–05	0.162E–05
112	0.771E–06	0.771E–06	0.771E–06	0.771E–06

The evolution of optical and microphysical properties of aerosols during their diffusion sinking from 90-km altitude is illustrated in Figs. 1–4. Considered is the case of strong turbulent mixing with $D = 5.5$ m^2/s. Time behavior of the accumulative and coarse fractions were simulated at each altitude within the anomalous layer using three aerosol subfractions with modal radii $r_{im} = 0.5\, r_m$, r_m, and $2.0\, r_m$; The parameters f_i and b_i were adjusted in such a way that the three subfractions combined were optically equivalent to the initial distributions in the two fractions adopted.

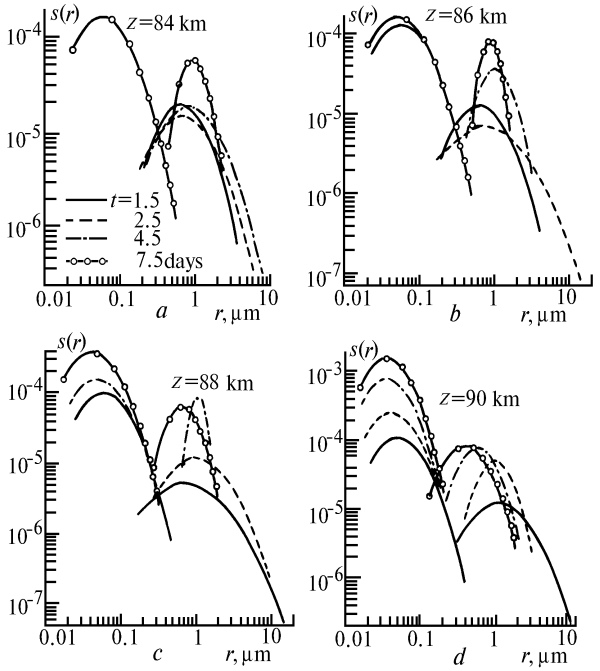

FIG. 1. Time evolution of distribution mode and width for the coarse aerosol fraction.

Shown in Fig. 1 are the results of calculating the size spectra for the two fractions. Spectra widths and modes were monitored in time for four altitudes z = 84, 86, 88, and 90 km. Spectrum evolution was monitored from 1.5 to 7 days after the injection.

Time invariance of size spectrum for microdisperse fraction at 84-km altitude is because the initial altitude of aerosol anomaly was taken at 95 km. As numerical estimates show, sedimenting particles of this fraction reach 86-km altitude only the 7th day after (Fig. 1*b*), while 88 and 90 km — the fourth and second days, respectively.

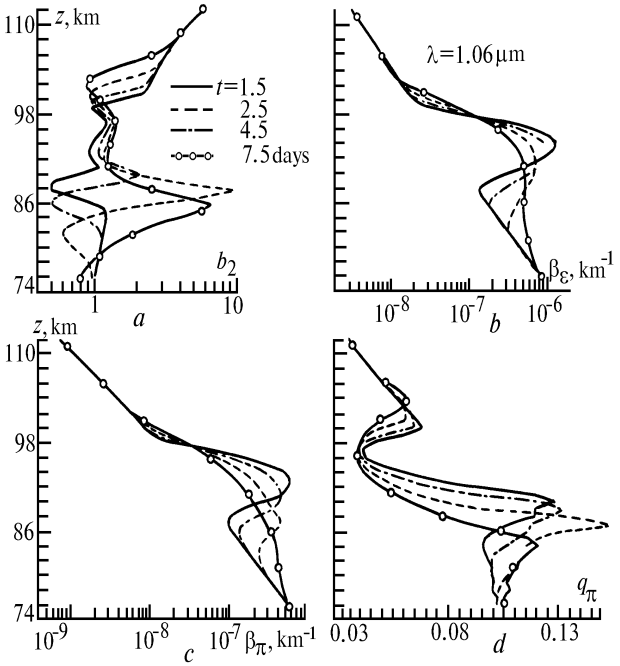

FIG. 2. Time evolution of vertical profiles of aerosol scattering parameters for the wavelength $\lambda = 1.06$ *μm: distribution width of coarse fraction* $b_2(z)$ *(a), extinction coefficient* $\beta_\varepsilon(z)$ *(b), backscattering coefficient* $\beta_\pi(z)$ *(c), and the lidar ratio* g_π *(d).*

The situation is quite different for the coarse aerosol fraction changing at all altitudes in both the spectrum mode and width. Specifically, the spectrum substantially changes in width at 84, 86, and 88 km, while becoming smaller-sized toward 90-km altitude.

Time evolution of $b_2(z, t)$, the distribution width of the coarse fraction, is shown in Fig. 2*a* in detail, from which it is seen that the size spectrum typical for the altitudes of the initial injection evolves to a substantially broader one with time. Also, the separation of aerosol particles due to gravity, initially important at altitudes just below the original anomalous layer, expands with time downward.

While differing in detail, both profiles of extinction and backscattering coefficients show, on the whole, quite slow spread of the anomalous aerosol layer downward. On the contrary, lidar ratio (Fig. 2*d*), owing to the sedimenting anomalous layer, experiences strong variations, up to 300–400%, and, as the estimates show and unlike the extinction

coefficient in Fig. 2*b*, has value controlled considerably by the range of variation of the coarse fraction.

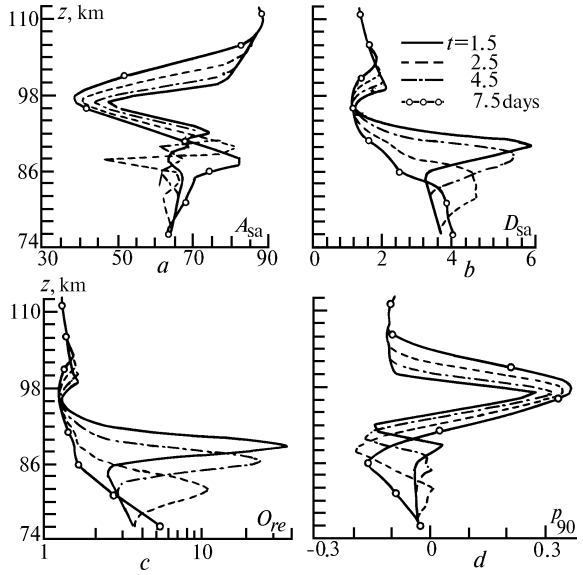

FIG. 3. Time evolution of vertical profiles of the parameters accounting for the shape of scattering phase function and the degree of polarization at the scattering angle 90°, *for the wavelength* λ = 1.06 μm*: $A_{sa}(z)$ (a), $D_{sa}(z)$ (b), $O_{re}(z)$ (c), and $p(90, z)$ (d).*

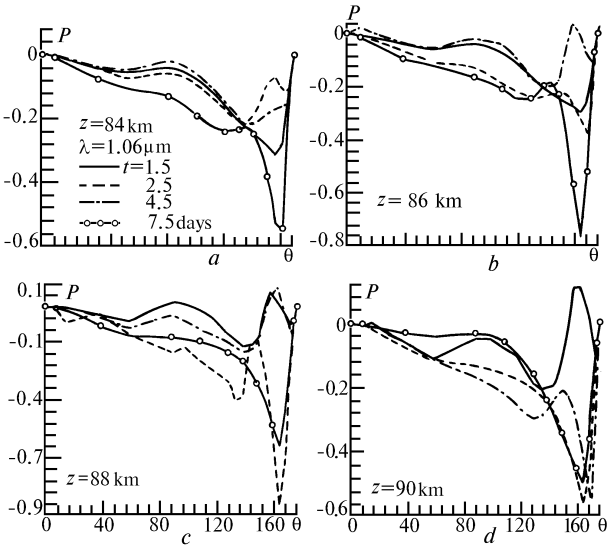

FIG. 4. Time evolution of angular dependence of the polarization degree $p(\theta, z)$ in the process of turbulent spreading and sedimentation of the mesospheric anomalous layer.

More complicated pattern is evident for the scattering phase function, from changes in its parameters describing forward peak, $A_{sa} = \mu(15°)/\mu(110°)$, Fig. 3*a*, backward peak $D_{sa} = \mu(165°)/\mu(110°)$, Fig. 3*b*, aureole peak, $O_{re} = \mu(0°)/\mu(5°)$, Fig. 3*c*, as well as the degree of polarization at the angle θ = 90°, Fig. 3*d*.

As computations show (Fig. 3*a*), there is accumulation of relatively small aerosol particles just above the anomalous layer, which leads to much less forward peaked phase function, although not to that of the Rayleigh type. Peak in D_s profile in Fig. 3*b* gradually shifts, downward, a feature characteristic of strong variations in the content of coarse aerosol fraction at those altitudes. The same feature is apparent from the results in Fig. 3*c* for the aureole portion of the phase function. The degree of polarization at the angle θ = 90° closely follows the altitude behavior of $A_{sa}(z)$, the parameter responsible for overall asymmetry of the phase function.

Figure 4 illustrates angular transformation of the degree of polarization at the wavelength λ = 1.06 μm, which, as was already noted above, is dominated by the variability of the coarse aerosol fraction at each altitudes in the case considered.

It should be noted in conclusion, that, as the results presented show, the rate and character of structural change incurred in mesospheric aerosol essentially depend on the process input parameters - background aerosol profile, strength of turbulent mixing, characteristic size of injected aerosol particles, and density of aerosol matter - all those determining the specific behavior of the aerosol optical properties. In particular, the above results are specialized to the case of increased concentration of coarse aerosol fraction, what determinated the behavior of the degree of polarization, $p(\theta, z)$.

With the availability of such a multiparametric model, we shall continue the comprehensive study of many factors of mesospheric aerosol variability by constituently analyzing their individual impacts.

ACKNOWLEDGMENTS

The author sincerely appreciates the support from Russian Foundation for Fundamental Researches (Grant No. 94-05-16463-a).

REFERENCES

1. V.N. Lebedinets, *Aerosol of the Upper Atmosphere and Cosmic Dust* (Gidrometeoizdat, Leningrad, 1981), 272 pp.
2. V.N. Lebedinets, *Dust in the Upper Atmosphere and Outer Space, Meteors* (Gidrometeoizdat, Leningrad, 1980), 248 pp.
3. R.F. Rakhimov, Atm. Opt. **4**, No. 6, 470–473 (1991).
4. R.F. Rakhimov, Atmos. Oceanic Opt. **5**, No. 5, 343–347 (1992).
5. P. Reist, *Introduction to Aerosol Science* (Collier McMillan Publishers, London, 1984).
6. V. Webb, *Structure of Stratosphere and Mesosphere* [Russian translation] (Mir, Moscow, 1969), 259 pp.

7. A.E. Mikirov and V.A. Smerkalov, *Study of Scattered Radiation in the Upper Atmosphere* (Gidrometeoizdat, Leningrad, 1981), 208 pp.
8. M. Grinberg, *Cosmic Dust* [Russian translation] (Mir, Moscow, 1970), 200 pp.
9. A.P. Grinin and F.M. Kuni, Tr. Ins. Exp. Meteorol., Akad. Nauk SSSR, Obninsk, No. 35(113), 52–56 (1985).